Single Crystals of L-*O*-Serine Phosphate X-Irradiated at Low Temperatures: EPR, ENDOR, EIE, and DFT Studies

Kjell Tage Øhman,* Audun Sanderud, Eli Olaug Hole, and Einar Sagstuen

Department of Physics, University of Oslo, P.O. Box 1048 Blindern, NO-0316 Oslo, Norway

Received: February 28, 2006; In Final Form: May 23, 2006

Single crystals of the phosphorylated amino acid L-*O*-serine phosphate were X-irradiated and studied at 10 K and at 77 K using EPR, ENDOR, and EIE techniques. Two radicals, R1(10 K) and R1(77 K), were detected and characterized as two different geometrical conformations of the protonated reduction product >CH−$\dot{C}(OH)_2$. R1(10 K) is only observed after irradiation at 10 K, and upon heating to 40 K, R1(10 K) transforms rapidly and irreversibly into R1(77 K). The transition from R1(10 K) to R1(77 K) strongly *increases* the isotropic hyperfine coupling of the $\dot{C}-CH_\beta$ coupling (Δ = 32 MHz) and the major $\dot{C}-OH_\beta$ coupling (Δ = 47 MHz), in sharp contrast to the their much *reduced* anisotropic hyperfine couplings after the transition. An umbrella-like inversion of the carboxylic acid center, accompanied by minor geometrical adjustments, explains the changes of these observed isotropic and anisotropic couplings. DFT calculations were done on the reduced and protonated L-*O*-serine phosphate radical at the B3LYP/6-311+G(2df,p)//B3LYP/6-31+G(d) level of theory in order to support the experimental observations. Two different conformations of the anion radical, related by an inversion at the carboxylic center, could be found within the single molecule partial energy-optimization scheme. These two conformations reproduce the experimental hyperfine couplings from radicals R1(10 K) and R1(77 K). A third radical, radical R2, was observed experimentally at both 10 and 77 K and was shown to be due to the decarboxylated L-*O*-serine phosphate oxidation product, a conclusion fully supported from the DFT calculations. Upon thermal annealing from 77 to 295 K, radicals R1(77 K) and R2 disappeared and all three previously observed room-temperature radicals could be observed. No phosphate-centered radicals could be observed at any temperatures, indicating that the phosphate−ester bond break for one of the room-temperature radicals does not occur by dissociative electron capture at the phosphate group.

1. Introduction

The amino acid analogue L-*O*-serine phosphate (SP, Scheme 1) has been considered to be an appropriate model system for the study of radiation-induced processes leading to scission of the phosphate−ester bond in the DNA backbone structure. The reason is that SP has molecular and electronic properties functionally similar to, for example, a nucleotide.

In particular, the phosphate−ester group in SP models the sugar−phosphate junction in DNA, whereas the carboxylic group is known to behave as an effective electron scavenger much like the aromatic nucleotide bases in DNA.

A previous EPR/ENDOR-study on irradiated single crystals of SP at room temperature was published by Sanderud and Sagstuen.[1] These authors identified three different radical species stable at room temperature. Two of these species were a side-chain H-abstraction radical at C3 and a deaminated reduction product, both well-known secondary radicals in irradiated amino acids.[2] The third species was a carbon C3 centered radical formed by scission of the phosphate−ester bond on the amino acid side. Mechanisms for the formation of these three room-temperature radicals were discussed by Sanderud and Sagstuen.[1] Phosphate-centered radicals, formed from SP by ionizing radiation, have not been observed to date.[1]

In a recent paper, Lipfert et al. presented a detailed DFT study on the structure of radicals formed in L-*O*-serine phosphate.[3] The results provided conclusive support for the interpretations given in the experimental work.[1] In addition, Lipfert et al. investigated mechanisms for the formation of these radicals and presented theoretical evidence for the model proposed by Sanderud and Sagstuen,[1] that the third room-temperature species could originate from a primary reduction product. In particular, Lipfert et al.[3] demonstrated the possible existence for a phosphoranyl radical as an intermediate species in a phosphate−ester dissociative electron capture (DEC) process leading to the third room-temperature radical.

Because most primary radicals are observable only at temperatures below room temperature, EPR/ENDOR experiments of single crystals of SP irradiated at low temperatures are required in order to put the proposed mechanisms to test, thus establishing if a DEC process is feasible in this model system.

It is well-known that the primary amino acid reduction product, usually a protonated carboxyl anion radical, is pyramidal at the radical center.[4] However, only one of the possible pyramidal conformations has been observed in one given system. During the course of the present work, it was found that two of these conformations could be stabilized depending on the temperature at which the system was irradiated. Thus, a detailed experimental and DFT assisted analysis of the geometric, electronic, and energetic properties of the two conformations were made.

2. Experimental and Computational Methods

Single crystals of L-*O*-serine phosphate (SP) (Sigma-Aldrich) were grown from saturated aqueous solutions by slow evapora-

* Corresponding author. Kjell Tage Øhman, Department of Physics, University of Oslo, P.O. Box 1048 Blindern, NO-0316 Oslo, Norway; e-mail: k.t.ohman@fys.uio.no.

10.1021/jp061265o CCC: $33.50
Published on Web 07/14/2006

SCHEME 1: Molecular Structure and Crystallographic Geometry of L-*O*-Serine Phosphate (SP)

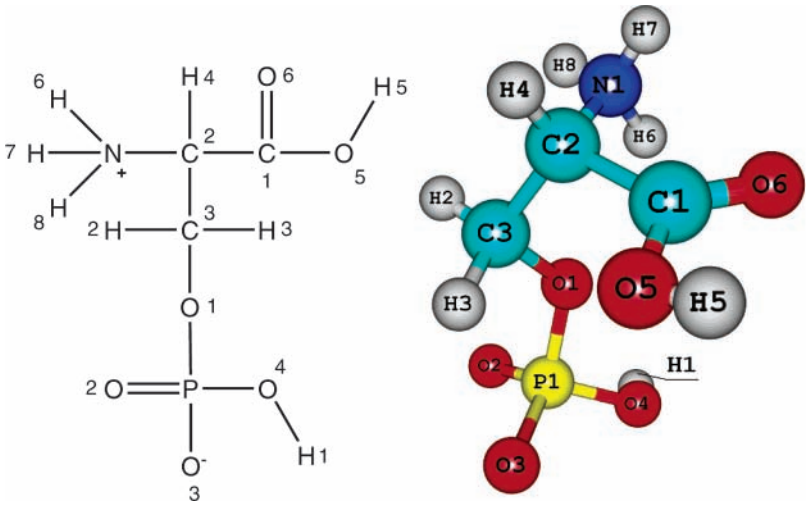

tion at 55 °C ("normal" crystals). Partially deuterated crystals of SP with the polar protons exchanged with deuterons were similarly prepared by crystallization from deuterium oxide (99%, Cambridge Isotope Laboratories).

Single crystals of SP are orthorhombic with space group symmetry $P2_12_12_1$, containing four molecules in the unit cell.[5] The crystallographic configuration of the SP molecule is shown in Scheme 1. The phosphate group is singly protonated and thus carries one formal negative charge, counterbalanced by a protonated amino group. The carboxyl group is formally neutral.

All polar protons and oxygen atoms except for O1 and O6 in the SP molecule are participating in external hydrogen bonding. Consequently, the C1−O5−H5 carboxyl fragment, the amino group, and the phosphate group are all firmly anchored in the crystalline environment. No internal hydrogen bonds are reported.[5]

Identification of the crystal axes was made using a Weissenberg X-ray diffraction camera, and aided by the diffraction pictures the rotation axis was aligned within 1° with one of the crystal axes. The crystals were subsequently transferred to copper sample holders without loss of alignment. The orthogonal Cartesian reference system in this work corresponds to the crystal axis system $\langle a,b,c \rangle$.

The sample holder was fitted to an Air Products HeliTran LT3 cryostat, which was cooled by liquid nitrogen/helium. The cryostat was inserted into a telescoping vacuum shield holding a TM_{011} EPR/ENDOR cylindrical cavity and with the crystal irradiation cabinet situated immediately above the cavity roof. A Philips chromium target tube operated at 50 kV/40 mA was used for X irradiation of the crystals at sample temperatures of about 10 K (liquid helium cryogen) and 77 K (liquid nitrogen cryogen) to a total dose of about 40 kGy. After irradiation, the crystals were lowered from the irradiation cabinet into the cavity for EPR/ENDOR/EIE measurements. This setup secures temperature stability between the irradiation and the measurement phase. A calibrated Oxford Instruments ITC 503 module with a thermocouple mounted to the base of the sample holder controlled the sample temperature during irradiation and measurements.

X-band EPR, ENDOR, and EIE spectra were obtained using a BRUKER EleXsyS 560 SuperX X-band spectrometer connected to a Linux workstation running BRUKER Xepr software. For ENDOR/EIE, the system was set to generate a square-wave frequency modulation of the rf field at 10 kHz with a modulation depth of typically 150 kHz. A 200-W 3200L ENI rf-amplifier was employed. For technical reasons, the ENDOR rf field could not be swept above about 45 MHz. For the EPR and ENDOR measurements, three different orthogonal planes of rotation were recorded at 5° intervals. A fourth plane skewed with respect to the crystal axes was recorded at the 77 K experiment to solve the Schonland ambiguity.[6]

The experiments will give four different hyperfine/quadrupolar tensors for each coupling atom due to the four SP molecules in the orthorhombic crystal unit cell. All tensors given in the tables represent the (x,y,z) molecule in the crystal cell[5] and the choice of the correct tensor for the (x,y,z) molecule is based on the discussion of the radical structure and the DFT calculations.

The proton and phosphorus hyperfine coupling (HCF) tensors were obtained from the experimental data using the MAGRES program.[7] The ^{14}N hyperfine and nuclear quadrupolar coupling (NQC) tensors were obtained using the NQENDFIT program.[8,9] These programs assume an isotropic g tensor, which proved to be a good approximation for this study of SP. Spectrum simulations were made using the program KVASAT as described previously.[10,11]

The DFT calculations were performed using the GAUSSIAN03 program package.[12] The fully or partially optimized radical geometries were obtained using the B3LYP hybrid functional[13−15] and the 6-31+G(d) basis set.[16] The subsequent single-point calculations of the hyperfine tensors on these geometries were done with the B3LYP hybrid functional and the 6-311+G(2df,p) basis set.[16] The B3LYP functional together with these Pople basis sets have been applied successfully to a number of biological radicals.[17]

An ONIOM calculation using standard semiemperical methods such as AM1 or PM3 cannot describe the hypervalent phosphate in SP properly,[18] and a full cluster approach was not feasible with our available computers. Hence, all calculations were performed on a single molecule at 0 K. The effects of the crystalline environment can to some extent be incorporated indirectly either by freezing some of the atomic coordinates during a geometry optimization or manually changing some of the atomic coordinates after a geometry optimization, thus simulating hydrogen bonding and various steric interactions. The single molecule approached with constrained optimization has been adopted previously by Vanhaelewyn et al. in order to determine radical conformations.[19] In combination with the *NoSymm* option of GAUSSIAN03, the eigenvectors (principal directions) of the calculated dipolar coupling principal values

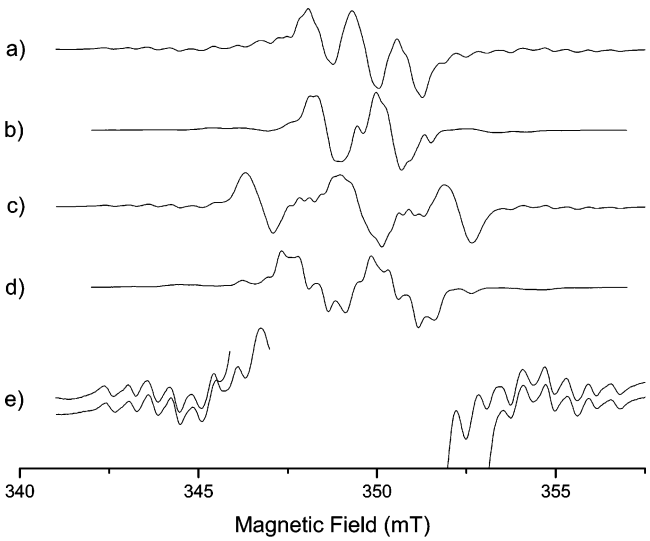

Figure 1. First-derivative EPR spectra (centered at $g_e = 2.0023$) of X-irradiated L-*O*-serine phosphate single crystals. (a) X irradiation and measurements at 10 K with nondeuterated (normal) crystals, (b) X irradiation and measurements at 10 K with deuterated crystals, (c) X irradiation and measurements at 77 K with normal crystal, and (d) X irradiation and measurements at 77 K with deuterated crystals. In e, both of the above nondeuterated spectra a and c are shown at 10X amplification (central part omitted) illustrating that the resonances flanking the central resonance are identical. All spectra are measured with the external magnetic field along the $\langle a \rangle$ axis.

are directly comparable with the experimental results. The atomic spin densities were obtained using natural population analysis.[20]

3. Experimental Results and Analysis

3.1. EPR Results. EPR spectra with the external magnetic field directed along the $\langle a \rangle$ axis from experiments at 10 and at 77 K are shown in Figure 1. In both cases using normal crystals, a dominating 1:2:1 type triplet resonance due to two nearly equal proton interactions is apparent in the center of the spectrum together with weaker and more complex resonances on each side of the triplet. The 77 K triplet resonance is much wider at all orientations of the external magnetic field as compared to the 10 K triplet resonance. The weak and complex resonances on each side of the triplets remain unchanged between the two experiments as shown in Figure 1e.

Figure 1b and 1d shows spectra corresponding to those in Figure 1a and 1c but using partially deuterated crystals. It is evident that the dominating triplets in both cases change into doublets. Clearly, one of the interactions contributing to the triplet resonances is due to an exchangeable proton. Similarly, the weaker flanking lines are also reduced in total width and complexity.

The resonances exhibit only very small g-factor variations and were assumed isotropic for the further analysis of coupling tensors.

3.2. ENDOR Results at 10 K. After X irradiation and measurements at 10 K, eight hyperfine coupling tensors (denoted nos. 1, 2, 3, 4, A, B, C, and D) were established from the ENDOR data and are reported in Tables 1 and 3. These hyperfine interactions could be ascribed to seven protons and one phosphorus atom. As illustrated in Figure 2, the magnetic field was locked at two distinctly different positions in the EPR spectrum (Figure 1a) in order to obtain all of the corresponding resonance lines. The hyperfine coupling tensors (nos. 1−4) were obtained with the magnetic field position locked to the dominating central EPR-resonance, and the hyperfine coupling tensors (nos. A−D) were obtained with the magnetic field position locked to one of the weak flanking EPR-resonance lines. Figure 2a and b shows the ENDOR spectra obtained with the external magnetic field directed along the $\langle a \rangle$ axis at these two different magnetic field position settings. The phosphorus resonance no. 5 and the nitrogen resonance no. E could not be followed through three orthogonal planes of rotation; hence, no coupling tensors from these two resonances could be established.

Experiments with X irradiation and measurements at 10 K using partially deuterated crystals clearly show that proton coupling nos. 2 and 3 are exchangeable, whereas proton coupling no. 1 is nonexchangeable. It was not possible to uniquely decide whether the proton couplings (nos. A−D) originate from exchangeable protons due to the low signal-to-noise ratio when the magnetic field was locked to the weak flank resonance lines of the EPR spectrum. Also, the Schonland ambiguity,[6] the sign-ambiguity of the nondiagonal elements in the coupling tensor, was not resolved by direct experiments at 10 K but was resolved indirectly by comparisons of the most probable radical geometry, the crystallographic directions and the DFT calculated tensors.

3.3. ENDOR Results at 77 K. After X irradiation and measurements at 77 K, five new hyperfine coupling tensors were established from the ENDOR data (nos. I−V in Figure 2c, for no. III see below) and are reported in Table 2. The magnetic field was locked at the center of the central EPR-resonance (Figure 1c). The hyperfine coupling tensors were ascribed to four proton interactions (nos. I−IV) and one nitrogen interaction (no. V). The nitrogen nuclear quadrupolar tensor was also established. Figure 2c shows the ENDOR spectra obtained at 77 K with the magnetic field directed along the $\langle a \rangle$ axis. X irradiation and measurements at 77 K using partially deuterated crystals showed that the proton coupling tensors nos. II−IV are due to exchangeable protons, whereas coupling nos. I and V are clearly nonexchangeable. Because it was not possible to distinguish the no. III resonance line from other resonances in the crowded distant proton region (12−17 MHz) of the ENDOR spectra throughout the $\langle b \rangle$-axis rotation plane, coupling no. III was assumed to be isotropic in this plane. The Schonland ambiguity of coupling tensors nos. I, II, IV, and V was completely resolved in a separate experiment using a skewed axis of rotation; the polar angles of the rotation axis were $\theta = 30°, \varphi = 0°$.

3.4. Radical R1(10 K) Characterization. EIE was used to assign the ENDOR resonance lines in Figure 2b to Radical R1-(10 K). As shown in Table 1, tensor nos. 1−3 can be characterized as β-proton tensors because of their prominent axial symmetry and moderately anisotropic eigenvalues. Tensor nos. 4 and 5 were characterized as very distant phosphorus atom hyperfine coupling tensors because the corresponding resonance lines are centered at the free phosphorus frequency ($\nu_P = 6.03$ MHz), and the tensors exhibit small isotropic values and small anisotropic axially symmetric eigenvalues.

In sharp contrast to the nonexchangeable proton tensor no. 1, the exchangeable proton tensor nos. 2 and 3 exhibit significantly larger anisotropic eigenvalues, which is typical for β-OH couplings. The β-OH anisotropy is larger in magnitude than normal carbon bonded β protons because the β-hydroxyl protons are closer to the radical center because of the shorter bonding lengths.

It follows that the only possible location for the majority of the unpaired spin must be at C1. A radical center on C1 will not give rise to any observable α-proton coupling, whereas one major nonexchangeable β-proton coupling would be expected.

TABLE 1: Experimental Hyperfine Coupling Tensors for Radical R1(10 K) in Single Crystals of L-*O*-Serine Phosphate X-Irradiated and Measured at 10 K and the DFT Computed Hyperfine Coupling Tensors for Model A[a]

tensor	principal values (MHz)	anisotropic values (MHz)	isotropic value (MHz)	eigenvectors ⟨*a*⟩	⟨*b*⟩	⟨*c*⟩
	53.71(3)	10.96		−0.098(1)	0.892(2)	−0.441(2)
*β*H (no. 1)	39.75(2)	−3.00	42.75	0.803(1)	−0.191(2)	−0.565(1)
exp	34.80(2)	−7.95		0.588(1)	0.409(2)	0.697(2)
	54.10	11.23		−0.022	0.860	−0.511
H4	37.38	−5.49	42.87	0.794	−0.295	−0.532
DFT	37.13	−5.74		0.608	0.417	0.676
	51.14(3)	20.11		−0.436(0)	0.801(7)	−0.411(1)
*β*H (no. 2)	22.31(3)	−8.72	31.03	−0.166(0)	0.377(4)	0.911(3)
exp	19.62(3)	−11.40		0.885(1)	0.465(0)	−0.032(7)
	56.94	20.63		−0.440	0.731	−0.522
H9	27.75	−8.56	36.31	−0.283	0.438	0.853
DFT	24.24	−12.07		0.852	0.523	0.014
	10.25(4)	15.84		0.220(2)	0.967(5)	0.130(2)
*β*H (no. 3)	−11.49(3)	−5.90	−5.59	0.918(2)	−0.160(2)	−0.363(1)
exp	−15.53(3)	−9.94		0.330(4)	−0.120(2)	0.923(2)
	17.95	22.93		0.137	0.950	−0.279
H5	−14.29	−9.31	−4.98	0.936	−0.216	−0.277
DFT	−18.60	−13.62		0.323	0.224	0.920
	3.79(3)	0.85		−0.950(5)	0.052(682)	0.306(636)
P (no. 4)	2.53(5)	−0.41	2.94	0.031(32)	0.997(130)	−0.074(−)
exp	2.49(4)	−0.45		0.309(15)	0.060(−)	0.949(158)
	−0.47	0.63		−0.891	0.224	0.395
P	−1.38	−0.28	−1.10	0.383	0.838	0.389
DFT	−1.45	−0.35		0.244	−0.498	0.832
P (no. 5) exp	*b*	*b*	∼ ±1[c]			

[a] Uncertainties are given at the 95% confidence level in the last digit(s) of the quoted values. [b] Anisotropy could not be properly resolved. [c] Isotropic eigenvalue estimated from ENDOR spectra with the external magnetic field aligned along the crystal axis.

The two observed *β*-hydroxyl protons can be ascribed to H5 and H9, where the latter is added to O6 after electron capture at the carboxylic group.

As shown in Table 4, the deviation of the eigenvector corresponding to the maximum anisotropic coupling of tensor no. 1 with the crystallographic vector between C1 and H4 is only 6° (10° if calculated using an eigenvector from a different tensor alternative that corresponds better to the DFT calculated tensor), whereas the corresponding deviation for tensor no. 3 (assigned to a coupling with H5) with the C1···H5 direction is 24°. The discrepancy for tensor no. 3 is most likely caused by a small amount of unpaired spin at O5, which is well known to occur in various carboxylic anions, especially when hydroxyl proton H5 is situated near the nodal surface of the unpaired spin at C1, as in the present case.[21,22] The hydrogen bonds O5−H5···O2* and O5···H6*−N* shown in Figure 3, where * indicates atoms of neighboring molecules, are probably an important factor for the stabilization of the H5−O5−C1 fragment during the electron capture and subsequent protonation of the carboxylic group.

Tensor no. 2 is necessarily due to an interaction with a covalently bonded proton at O6, a proton that is incoming from a neighboring molecule. The closest polar group is shown in Figure 3 and is the most probable proton donor of H9. This polar proton transfer is justified by the prospect of attaining charge balance at the carboxylic group after electron capture. Similar proton transfers are well-established for a variety of carboxylic anion compounds.[21−25]

Tensor no. 4 is a weak interaction with a phosphorus atom. As shown in Table 4, the eigenvector corresponding to the maximum anisotropic coupling is almost parallel to the crystallographic C1···P direction.

3.5. Radical R1(77 K) Characterization. EIE was used in order to assign the ENDOR resonance lines in Figure 2c to Radical R1(77 K). Tensor nos. I−III can be characterized as proton *β* tensors. The interaction yielding tensor no. IV is also a proton hyperfine coupling, but the magnitude of the anisotropic eigenvalue indicates a coupling to a nucleus more distant from the radical center.

As shown in Table 4, the eigenvectors corresponding to the maximum anisotropic coupling of tensor nos. I and 1 (R1(10 K)) exhibit considerable similarity; this may also be the case for the eigenvectors corresponding to maximum anisotropic coupling of tensor nos. III and 3 (R1(10 K)). Tensor nos. I and 1 (R1(10 K)) also share the property of being due to nonexchangeable protons, whereas tensor nos. III and 3 (R1(10 K)) share the property of being due to exchangeable protons. The latter property is also shared by tensor nos. II and 2 (R1(10 K)) as well as by tensor no. IV.

Coupling nos. II and III exhibit *β*-hydroxyl properties because of their large anisotropy as compared to coupling no. I, even if the anisotropy is significantly smaller as compared to that of tensor no. 2 of radical R1(10 K) (to be discussed further below). Thus, the exchangeability and nature of the major couplings unequivocally pinpoint the radical center of radical R1(77 K) to be C1, that is, the same as for radical R1(10 K). The conclusion must be that radical R1(77 K) is also a protonated carboxyl anion.

Tensor no. IV is probably a coupling to an amino proton (H6*, Figure 3) at a neighboring molecule in the crystalline environment because the direction of the C1···H6* contact and the eigenvector of tensor no. IV corresponding to maximum anisotropic coupling are nearly parallel, as shown in Table 5.

TABLE 2: Experimental Hyperfine Coupling Tensors and ^{14}N Quadrupolar Coupling Tensor for Radical R1(77 K) in Single Crystals of X-Irradiated and Measured L-*O*-Serine Phosphate at 77 K and the DFT Computed Hyperfine Coupling Tensors for Model B[a]

tensor	principal values (MHz)	anisotropic values (MHz)	isotropic value (MHz)	eigenvectors ⟨*a*⟩	⟨*b*⟩	⟨*c*⟩
	81.72(4)	6.75		−0.031(2)	0.888(7)	−0.460(3)
*β*H (no. I)	73.02(2)	−1.95	74.97	−0.362(0)	0.419(2)	0.833(5)
exp	70.18(2)	−4.79		0.932(1)	0.192(2)	0.308(6)
	74.14	8.08		0.067	0.868	−0.492
H4	63.22	−2.84	66.06	−0.511	0.453	0.730
DFT	60.82	−5.24		0.857	0.202	0.474
	91.49(2)	13.74		0.824(1)	−0.452(1)	−0.343(1)
*β*H (no. II)	73.00(2)	−4.75	77.75	0.454(1)	0.887(1)	−0.078(2)
exp	68.75(2)	−9.00		0.340(0)	−0.092(2)	0.936(0)
	85.65	10.40		0.885	−0.385	−0.261
H9	71.63	−3.62	75.25	0.448	0.855	0.262
DFT	68.47	−6.78		0.123	−0.349	0.929
	27.36(03)	18.48		0.115(2)	0.979(9)	0.167(11)
*β*H (no. III)	0.52(10)	−8.36	8.88	0.783(0)	0.014(3)	−0.622(2)
exp	−1.25(10)	−10.13		0.611(2)	−0.203(11)	0.765(9)
	22.86	18.38		−0.287	0.945	0.154
H5	−3.91	−8.39	4.48	0.456	0.277	−0.846
DFT	−5.52	−10.00		0.843	0.173	0.510
	9.12(4)	9.69		0.240(3)	0.201(436)	0.950(14)
H (no. IV)	−5.26(3)	−4.69	−0.57	0.031(4)	−0.979(9)	0.199(441)
exp	−5.56(5)	−4.99		0.970(1)	−0.018(111)	−0.242(88)
	8.78(1)	1.14		−0.504(8)	0.755(7)	0.420(6)
*β*N (no. V)	7.54(1)	−0.10	7.64	−0.606(10)	−0.656(8)	0.450(12)
exp hfc	6.60(1)	−1.04		0.615(8)	−0.027(11)	0.788(6)
	10.08	0.69		0.158	0.937	0.313
N	9.06	−0.33	9.39	−0.381	−0.235	0.895
DFT hfc	9.03	−0.36		0.911	−0.260	0.319
	0.447(4)	0.447		0.301(7)	0.466(5)	0.832(4)
*β*N (no. V)	−0.036(4)	−0.036		0.725(7)	0.454(9)	−0.517(7)
exp nqc	−0.411(4)	−0.411		−0.619(8)	0.759(6)	−0.201(7)

[a] Uncertainties are given at the 95% confidence level in the last digit(s) of the quoted values.

None of the intra-atomic contacts to exchangeable protons (H6, H7, and H8) exhibit similar agreement.

It is noted that the crystallographic torsion angle between the carboxyl group plane and the C1−C2−N plane is only 3°. Even when the C1 radical center becomes pyramidal upon radical formation, only a small isotropic coupling to the amino nitrogen would therefore be expected. The signs of the quadrupolar coupling tensor elements (no. V) are assigned in analogy with a comparable radical in L-*O*-serine phosphate at room temperature (radical II in ref 1). It appears that the direction for the maximum quadrupolar coupling deviates only 9.3° from the crystallographic C2−N direction. For radical II in ref 1, the corresponding angle was 10.8°. It is difficult to extract further useful structural information from the nitrogen hyperfine and quadrupolar coupling tensor no. V. This is basically due to the high sensitivity of the amino nitrogen hyperfine and nuclear quadrupolar coupling tensors for the unpaired spin in the nitrogen σ bonds.[1]

3.6. Radical R2 Characterization. No EIE spectra of good quality could be obtained when the external magnetic field was locked at the flanking EPR resonance lines depicted in Figure 1e. Regardless of this, however, tensor nos. A−E can only be assigned to one radical, designated radical R2. This follows from the EPR spectrum simulations to be described below because all of these tensors are required for R2 to reproduce the experimental spectra satisfactorily. Also, regardless where the external magnetic field is positioned at the broad flanking EPR resonances, the same ENDOR resonance lines are observed.

Because both radicals R1(10 K) and R1(77 K) have been identified as protonated carboxylic anions, it would for stoichiometric reasons be expected that the second radical R2 should be an oxidation product. Primary cationic radicals of amino acids are well known to undergo immediate decarboxylation after the initial oxidation event.[2] Lipfert et al.[3] did show that decarboxylation from the pristine SP cation proceeds without any activation energy. This decarboxylated radical will have the majority of its unpaired spin located at C2, creating a large number of resolvable proton interactions in accordance with the observed wide EPR-spectra (Scheme 3).

Tensor no. A can be characterized as due to a proton α-coupling, and tensor nos. B−D can be characterized as due to proton β couplings. The complete nitrogen hyperfine coupling tensor no. E could not be established because the corresponding resonance positions could only be observed with the external magnetic field aligned along the crystal axes.

After decarboxylation, the axis of a highly spin populated 2p(C2) orbital is anticipated to be close to the broken σ bond between C1 and C2. The amino and phosphate groups are firmly anchored through external hydrogen bonding; thus, they contribute to stabilization of the radical in a conformation close to crystallographic structure.

Assuming that the unpaired spin is mainly located at C2, tensor no. A must be due to an interaction with H4. As shown in Table 6, the deviation between the eigenvector of the intermediate principal value of tensor no. A and the crystallographic C2−C1 direction is 8°. The angle between the

TABLE 3: Hyperfine Coupling Tensors for Radical R2 in Single Crystals of X-Irradiated L-*O*-Serine Phosphate and Measured at 10 K and the DFT Computed Hyperfine Coupling Tensors for Model C[a]

tensor	principal values (MHz)	anisotropic values (MHz)	isotropic value (MHz)	eigenvectors ⟨*a*⟩	⟨*b*⟩	⟨*c*⟩
	−104.66(6)	−38.60		0.831(1)	0.239(2)	0.503(1)
αH (no. A)	−63.19(23)	−2.87	−66.06	−0.249(1)	0.967(0)	−0.048(2)
exp	−30.33(7)	35.73		−0.498(1)	−0.086(1)	0.863(0)
	−97.31	−39.04		0.803	0.301	0.514
H4	−59.63	−1.36	−58.27	−0.206	0.950	−0.234
DFT	−17.87	40.40		−0.559	0.082	0.825
	49.48(3)	11.64		0.039(1)	0.044(2)	0.998(27)
*β*H (no. B)	32.56(4)	−5.28	37.84	0.998(2)	0.039(27)	−0.041(2)
exp	31.49(5)	−6.35		0.040(0)	−0.998(1)	0.043(2)
	42.33	11.37		0.111	0.286	0.952
H6	25.70	−5.26	30.96	0.703	−0.700	0.129
DFT	24.85	−6.11		0.703	0.655	−0.278
	101.83(4)	10.03		0.157(1)	0.809(3)	0.566(2)
*β*H (no. C)	89.67(2)	−2.13	91.80	0.587(1)	−0.537(2)	0.605(2)
exp	83.89(2)	−7.91		0.794(2)	0.237(2)	−0.560(3)
	109.34	9.74		0.337	0.736	0.588
H8	95.59	−4.01	99.60	0.388	−0.677	0.625
DFT	93.87	−5.73		0.858	0.017	−0.514
	22.38(3)	10.73		0.858(1)	0.213(20)	0.467(2)
*β*H (no. D)	6.61(4)	−5.04	11.65	0.028(1)	0.888(2)	−0.458(35)
exp	5.96(3)	−5.69		−0.513(1)	0.406(30)	0.756(18)
	26.22	11.41		0.795	0.286	0.534
H7	9.75	−5.06	14.81	0.041	0.854	−0.518
DFT	8.46	−6.35		−0.605	0.434	0.668
	23.91	9.64		0.869	0.233	0.437
H3	9.88	−4.39	14.27	0.130	0.745	−0.654
DFT	9.03	−5.24		−0.478	0.625	0.617
αN (no. E)	*b*	*b*	± (6...10)[c]			
exp						
	−6.53	0.59		0.176	0.933	0.313
N	−7.28	−0.16	−7.12	0.476	−0.359	0.803
DFT	−7.55	−0.43		0.862	0.008	−0.508
	167.33	8.60		0.844	−0.532	0.069
H2	155.63	−3.10	158.73	0.533	0.846	−0.009
DFT	153.23	−5.50		−0.053	0.044	0.998

[a] Uncertainties are given at the 95% confidence level in the last digit(s) of the quoted values. [b] Anisotropy could not be properly resolved. [c] Isotropic eigenvalue estimated from ENDOR spectra with the external magnetic field aligned along the crystal axis.

eigenvector of the largest principal value of tensor no. A and the C2−H4 direction is 11°. The C2 center, sp^3 hybridized before oxidation, would be expected to rehybridize to a more planar sp^2 structure after decarboxylation. The McConnell relation[26] with $Q = -73.4$ MHz[27] and the experimental isotropic eigenvalue of tensor no. A indicates 0.90 spin density at C2. Using the anisotropic eigenvalues of the hyperfine coupling tensor no. A, the Gordy−Bernhard relation[28,29] with $Q^z_{dip} = 38.7$ MHz indicates 0.93 spin density at C2. This small difference suggests that the C2 center is nearly completely sp^2 rehybridized.[30]

The isotropic *β*-proton coupling is described by the Heller−McConnell relation[31]

$$a_{iso}(CH_\beta) = (B_0 + B_2 \cos^2\theta)\rho^\pi \qquad (1)$$

where B_0 and B_2 are constants typically close to 0 MHz and 126 MHZ, respectively, for a planar CCH_β radical,[32] and for a planar CNH_β fragment about −4 and 118 MHz, respectively.[33] θ is the dihedral angle between the C−H_β or N−H_β bond and the axis of the 2p(C) orbital with spin density ρ^π.

From the crystallographic data,[5] the dihedral angles between the N−H6, N−H7, and C3−H3 directions and the C2−C1 direction are about 60°. Consequently, the isotropic eigenvalue for H6, H7, and H3 should be small. The isotropic value of tensor no. B is 37.8 MHz, and Table 7 shows that the crystallographic C2···H6 direction is close to the eigenvector of tensor no. B corresponding to maximum dipolar coupling, the C2−H7 and C2−H3 directions cosines on the other hand show no such correspondence.

Tensor no. C exhibits a large isotropic value of 91.8 MHz, which implies a dihedral angle close to 0°. This excludes the *β* protons H3, H6, and H7 as discussed above. The directions C2−H2 and N−H8 both have dihedral angles to the C1−C2 direction close to 0°, but as shown in Table 7 only the C2−H8 direction is in accordance with the eigenvector for the maximum dipolar coupling of tensor no. C.

Tensor no. D exhibits a small isotropic value of 11.7 MHz, and as discussed above *β* protons H6, H7, and H3 are all possible candidates for the proton responsible for coupling tensor no. D. From Table 7, both H3 and H7 remain as candidates. H3 and H7 could, in principle, be distinguished by an experiment using a deuterated crystal of SP, but because of the poor signal-to-noise ratio, this was not achieved. The anisotropic elements of nos. B−D are all quite similar and almost identical to those of the amino proton couplings of the structurally similar

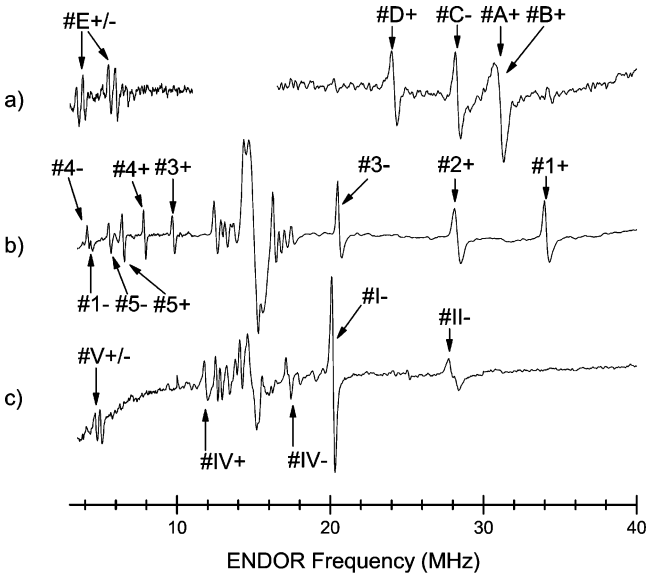

Figure 2. First derivative ENDOR spectra of X-irradiated L-*O*-serine phosphate single crystals with the external magnetic along the ⟨*a*⟩ axis. (a and b) X irradiation and measurements at 10 K. In a, the magnetic field is locked to a resonance line at the outer flank in the EPR spectrum of Figure 1a, whereas in b the field is locked to the central line. (c) X irradiation and measurements at 77 K. The magnetic field is locked to the central resonance line of the EPR spectrum in Figure 1c. The assignment of + or − to each ENDOR line indicates whether the corresponding nuclear transition belongs to the $m_s = +1/2$ or the $m_s = -1/2$ energy level manifold.

TABLE 4: C1−H4, C1−H5, and C1−P Crystallographic Directions of L-*O*-Serine Phosphate Compared with Selected Experimental Eigenvectors Corresponding to the Maximum Anisotropic Coupling of the Tensors from the R1(10 K) and R1(77 K) Radicals

crystallographic directions		experimental		angular deviation	
	C1−H4	no. 1	no. I	no. 1	no. I
⟨*a*⟩	0.056	+/−0.098	+/−0.031		
⟨*b*⟩	0.852	0.892	0.888	6°/10°	4°/6°
⟨*c*⟩	−0.520	−0.441	−0.460		
	C1−H5	no. 3	no. III	no. 3	no. III
⟨*a*⟩	0.083	0.220	0.115		
⟨*b*⟩	0.859	0.967	0.979	24°	21°
⟨*c*⟩	0.505	0.130	0.167		
	C1−P	no. 4		no. 4	
⟨*a*⟩	−0.944	−0.950		8°	
⟨*b*⟩	0.187	0.052			
⟨*c*⟩	0.272	0.306			

major room-temperature radical in glycine[34] and the R2 radical in alanine.[33] In the latter case, the isotropic couplings are also similar in magnitude to those of nos. B−D. Thus, it is tentatively suggested that all these three proton interactions in the L-*O*-serine phosphate radical R2 are due to the amino protons.

3.7. Configuration of Radical R1(10 K) and Radical R1-(77 K). As discussed in earlier sections, the radicals R1(10 K) and R1(77 K) are both assigned to a protonated carboxylic reduction product (anion) with the major part of the unpaired spin located at C1. Upon thermal annealing from 10 K, radical R1(10 K) is observed to transform irreversibly at 40 K to radical R1(77 K). This shows that R1(10 K) is the primary reduction product and second, that the R1(77 K) radical, which has the same radical center on C1, is a geometrically different and presumably energetically more stable conformation of the R1-

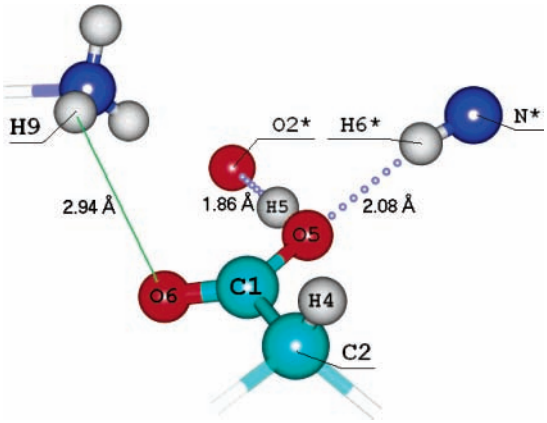

Figure 3. Illustration of the hydrogen bonds O5−H5···O2* and O5···H6*−N*, and the neighboring amino group, which is most likely the donor of the incoming proton at O6 after electron capture. Hydrogen bond lengths and the H9−O6 distances are given in angströms. Color coding: C, magenta; H, grey; O, red; N, blue.

TABLE 5: C1−H6, C1−H6*, C1−H7, and C1−H8 Crystallographic Directions of L-*O*-Serine Phosphate Compared with the Experimental Eigenvector Corresponding to the Maximum Anisotropic Coupling of Tensor no. IV of the R1(77 K) Radical[a]

experimental	crystallographic directions				
	no. IV	C1−H8	C1−H7	C1−H6	C1−H6*
⟨*a*⟩	0.240	−0.058	−0.443	0.042	0.23
⟨*b*⟩	0.201	−0.976	−0.841	−0.770	0.30
⟨*c*⟩	0.950	0.212	−0.312	−0.637	0.93

[a] H6* belongs to a neighboring molecule in the crystalline environment.

SCHEME 2: Chemical Structures of Radicals R1(10 K) and R1(77 K)

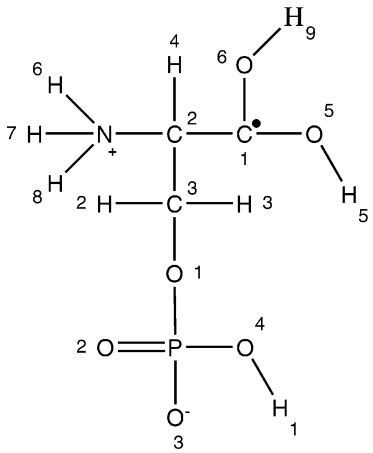

(10 K) radical. To understand the geometrical differences between R1(10 K) and R1(77 K), the similarities and differences between the hyperfine coupling tensor nos. 1−3 from radical R1(10 K) and hyperfine coupling tensor nos. I−III from radical R1(77 K) must be examined.

The differences between the eigenvectors corresponding to the maximum anisotropic eigenvalue of tensor nos. 1 and I due to H4, and between tensor nos. 3 and III due to H5 are small. This suggests that proton H4 and the fragment −O5−H5 do not move to any large extent between the two radicals. For H5, this can be understood in terms of the two hydrogen bonds in which the fragment −O5−H5 participates (see Figure 3). H4 is stabilized indirectly by extensive hydrogen bonding to the environment at the amino and the phosphate groups. However,

SCHEME 3: Chemical Structure of Radical R2

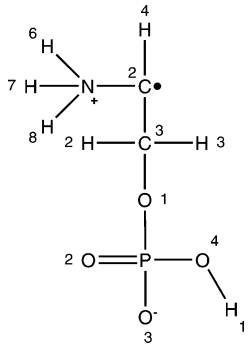

TABLE 6: C2−H4 and C2−C1 Crystallographic Directions of L-*O*-Serine Phosphate Compared with the Experimental Eigenvector Corresponding to the Maximum Anisotropic Coupling, A(max), of Tensor no. A of Radical R2 and the Intermediate Anisotropic Coupling, A(int), of Tensor no. A from Radical R2

	experimental	crystallographic	angular deviation
	no. A(max)	C2−H4	
⟨*a*⟩	−0.498	−0.442	
⟨*b*⟩	−0.086	−0.276	11°
⟨*c*⟩	0.863	0.853	
	no. A(int)	C2−C1	
⟨*a*⟩	−0.249	−0.188	
⟨*b*⟩	0.967	0.965	8°
⟨*c*⟩	−0.048	−0.183	

TABLE 7: Various C2−H Crystallographic Directions of L-*O*-Serine Phosphate Compared with the Experimental Eigenvector Corresponding to the Maximum Anisotropic Coupling of Tensor nos. B−D of the R2 Radical

	experimental			crystallographic directions				
	no. B	no. C	no. D	C2−H2	C2−H3	C2−H6	C2−H7	C2−H8
⟨*a*⟩	−0.039	−0.157	0.858	0.800	0.897	−0.095	−0.740	−0.251
⟨*b*⟩	−0.041	−0.809	0.213	−0.590	0.241	−0.227	−0.371	−0.828
⟨*c*⟩	−0.998	−0.566	0.467	0.111	0.370	−0.969	−0.561	−0.501

a difference exists between the eigenvectors corresponding to the maximum anisotropic eigenvalue of tensor nos. 2 and II due to H9. The atom O6, which is covalently bonded to H9 after protonation, does not participate in any strong hydrogen bond[5] and consequently the geometry of the fragment −O6−H9 should be less geometrically stable then the fragment −O5−H5. Nevertheless, from crystallographic data the donating amino group is situated very much out the carboxylic plane and before protonation the dihedral angle O5−C1−O6−H9 is 55° (Figure 3). It therefore seems reasonable to assume that after radical formation and protonation of O6, H9 is situated out of the O5−C1−O6 plane to a large extent in both R1(10 K) and R1(77 K) and furthermore situated on the same side of the carboxylic group as H4 (Figure 4).

Tensor nos. I and II have considerably smaller anisotropic couplings and much larger (almost by a factor of 2) isotropic values, as compared to tensor nos. 1 and 2. Tensor no. III compared to tensor no. 3, however, shows the opposite trend, but to a much smaller extent.

These features of the couplings can be understood by realizing that the carboxylic group of the protonated anion in fact is pyramidal, and that the majority of the unpaired spin resides in a sp^2 hybrid orbital on C1. This implies that the spin density is larger on one side of the plane of the carboxylic group (the major spin lobe) and smaller on the opposite side (the minor spin lobe). Such pyramidal configurations are known to exist from a number of previous studies of carboxylic acid and amino acid anions.[4]

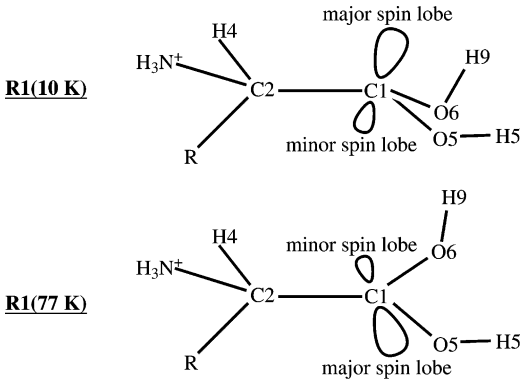

Figure 4. Schematic illustration of the carboxylic group configurations for radicals R1(10 K) and R1(77 K). The major and minor spin lobes switch sides upon the transition from radical R1(10 K) to radical R1-(77 K).

A β proton located on the same side (here designated as a cis conformation) as the major spin lobe gives larger anisotropic couplings than if the β proton is located on the opposite side (trans conformation) due to smaller distance between the proton and the average unpaired spin (see Figure 4 for an illustration). It is also known that the isotropic value is reduced when a β proton is in a cis conformation as compared to the trans conformation,[4] contrary to the behavior of the anisotropic coupling. For protonated carboxylic acid anions, the isotropic coupling value for a carbon bonded β proton has been described by a modified version of the Heller−McConnell relation[4]

$$a_{\mathrm{iso}}(\mathrm{CH}_\beta) = B_2 \cos^2\theta \qquad (2)$$

with B_2 in the range of 78−92 MHz for the trans configuration and 36−46 MHz for the cis configuration, whereas for a hydroxylic β proton the corresponding relation is

$$a_{\mathrm{iso}}(\mathrm{OH}_\beta) = -4 + B_2 \cos^2\theta \qquad (3)$$

with $B_2 = 61$ MHz for a trans configurations and 43 MHz for a cis configuration. The dihedral angle between the O−H_β or C−H_β bond and the axis of the spin populated sp^2 orbital at the radical center is given by θ.

The experimental isotropic eigenvalues of the tensor nos. 1 (R1(10 K)) and I (R1(77 K)) due to H4 are 42.8 and 75.0 MHz, respectively. Using the normal vector to the crystallographic carboxyl plane as an approximation to the axis of the spin lobe, the crystallographic dihedral angle between the C2−H4 bond and the axis of the spin lobe is 29°. Considering eq 2 with this dihedral angle together with an inversion of the carboxylic group from a cis to a trans pyramidal conformation, the changes in the isotropic eigenvalues from 10 to 77 K can readily be understood. This will also be consistent with the anisotropic eigenvalue of no. 1 being larger than the anisotropic eigenvalue of no. I, 11.0 and 6.8 MHz, respectively.

The experimental isotropic values of tensor nos. 2 (R1(10 K)) and II (R1(77 K)) due to H4 are 31.0 and 77.8 MHz, and the maximum anisotropic eigenvalues of tensor nos. 2 and II are 20.1 and 13.7 MHz, respectively. These eigenvalues exhibit the same trend when going from R1(10 K) to R1(77 K) as discussed for the tensors due to H4. There is no well-defined crystallographic dihedral angle for the incoming proton H9, but eq 3 indicates a large overlap between the O6−H9 bond and

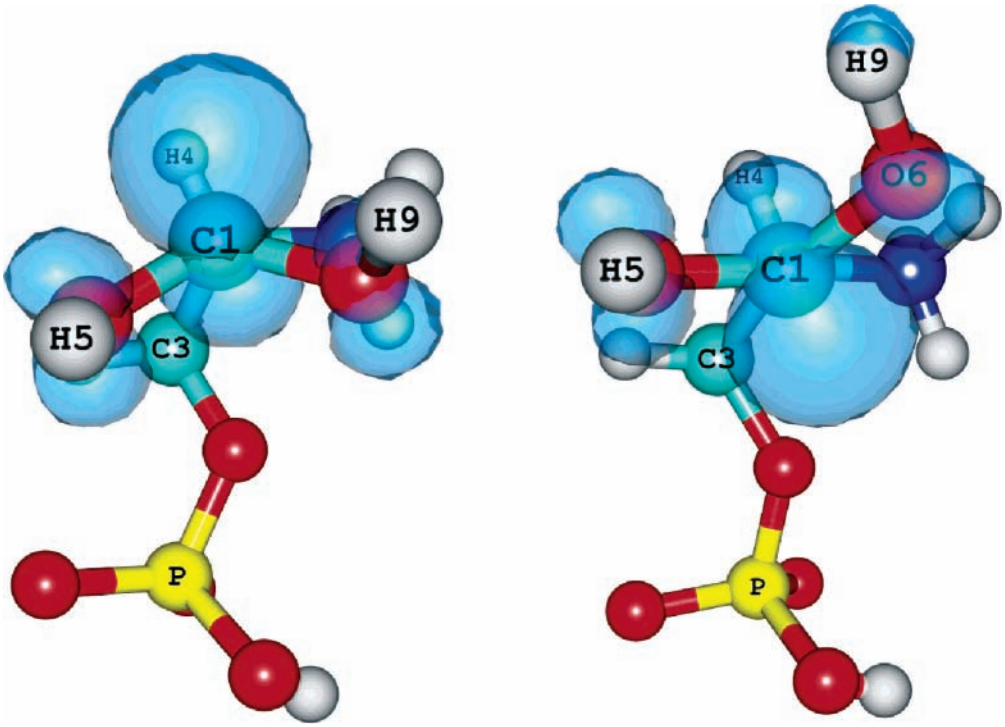

Figure 5. Model A (left) and model B (right) are mimicking the molecular conformations of the R1(10 K) and R1(77 K) radicals, respectively, formed by X irradiating L-*O*-serine phosphate crystals at 10 and 77 K. The transparent shade of blue color is the calculated positive spin density isosurface at the 0.0054 au contour. The geometries are viewed along the C1−C2 bond. Color coding: C, magenta; H, grey; O, red; N, blue; P, yellow.

the major/minor spin lobe in R1(10 K)/R1(77 K), respectively. This is also consistent with the out-of-carboxylic plane position of the proton-donating amino group as discussed earlier.

The second hydroxyl proton H5, responsible for hyperfine coupling tensor nos. 3 (R1(10 K)) and III (R1(77 K)), exhibits the opposite trend concerning isotropic and anisotropic values, as compared to the tensors for the H4 and H9 protons. This can be understood by the fact that H5 prior to electron capture is close to the carboxylic plane O6−C1−O5, participating in a hydrogen bond (Figure 3). Because the isotropic values of tensor nos. 3 and III are small, H5 must remain close to the O6−C1−O5 plane and thereby to the spin nodal surface in both anion radicals. Consequently, there can be no major changes in the unpaired spin distribution near H5 as compared to the H4 and H9 protons, and no genuine cis or trans configuration can be assigned to H5 in R1(10 K) and R1(77 K). Hence, an inversion will not alter the eigenvalues of tensor nos. 3 and III significantly. Taking other small geometrical changes between the radicals R1(10 K) and R1(77 K) into account, the differences between tensor nos. 3 and III do not appear unreasonable.

4. Density Functional Theory (DFT) Calculations

4.1. Optimization Procedure and Hyperfine Tensor Calculations of Radical R1(10 K) and R1(77 K). The partially optimized radical geometries A and B in Figure 5, mimicking the molecular conformations of radicals R1(10 K) and R1(77 K) respectively, were obtained through multiple steps. The computationally demanding phosphate group was removed from a SP molecule and replaced with hydrogen. After electron addition, a proton (H9) was covalently bonded to O6 making the net charge of the radical +1, analogous to a doubly protonated alanine anion. This molecule was then fully optimized with slightly different initial values for the torsion angle of the planar carboxylic group. As shown in Figure 6, this resulted in three major structures distinguished by the pyrimidalization of the carboxylic group. The structure on the left in Figure 6 has the major spin lobe on the same side as H4, which is also the case for radical R1(10 K); and the structure on the right in Figure 6 has the major spin lobe on the opposite side of H4, which is the case for radical R1(77 K). These two structures represent the basis for models A and B (Figure 5), which in turn yield the calculated hyperfine coupling tensors for radical R1(10 K) included in Table 1 and for radical R1(77 K) included in Table 2. To proceed from the left and right structures in Figure 6 to models A and B in Figure 5, the phosphate group was put back onto the molecule as close to the crystallographic structure as possible. Next, the carboxylic group is rotated actively around the C1−C2 bond until a satisfactorily isotropic eigenvalue for H4 is achieved, as compared with experimental data. Similarly, the positions for hydroxyl protons H5 and H9 are changed actively, by modifying the dihedral angles H5−O5−C1−C2 and H9−O6−C1−C2, until satisfactorily isotropic eigenvalues are achieved.

Between the iterations these dihedral angles were sometimes frozen followed by a partial optimization of the molecular geometry. Usually the numerical computation of isotropic hyperfine coupling constants have lower accuracy than the anisotropic coupling constants;[35] however, the isotropic hyperfine couplings of the β protons considered here are much more sensitive to these dihedral changes, thus making it easy to evaluate the different geometries. Also in combination with the procedures above, minimizing the Frobenius matrix norm of the difference between the experimental tensor and the calculated tensor was used as a tool for finding a good match for the entire tensor, not only the isotropic eigenvalue. The Frobenius matrix norm is defined as

$$||A||_F = \sqrt{\sum_{i=1}^{m}\sum_{j=1}^{m} |a_{ij}|^2}$$

for a symmetrical m-dimensional matrix A.

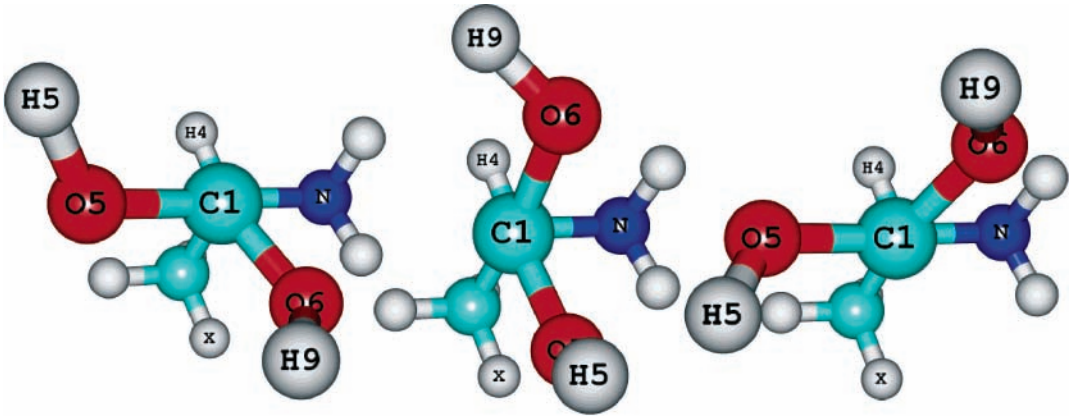

Figure 6. Three different optimized conformations of the doubly protonated alanine anion with respect to the pyrimidalization of the carboxylic group. The x atom is the hydrogen that has replaced the phosphate group. The geometries are viewed along the C1−C2 bond. Color coding: C, magenta; H, grey; O, red; N, blue.

The calculated hyperfine couplings for nos. 1, I, 2, and II of models A and B show the same magnitude relations between the anisotropic and the isotropic values as the experimentally values from radicals R1(10 K) and R1(77 K), as a consequence of the position of the major and minor spin lobes. Also, all three computed eigenvectors for nos. 1, I, 2, and II tensors exhibit acceptable similarity with the eigenvectors of the experimental tensors. However, the calculated anisotropic couplings for nos. 3 and III (H5) do not follow this trend as closely. As discussed earlier, the hydroxyl proton H5 is positioned close to the nodal surface of the unpaired spin and will therefore be influenced by an inversion of the carboxylic group to lesser extent. The DFT calculation confirms this assumption as the changes in anisotropic couplings between nos. 3 and III are far smaller than those between nos. 2 and II, which also is due to a hydroxyl proton. The calculated spin density at C1 was 0.75 for both model A and model B.

As can be seen directly from Figure 5, model A (R1(10 K)) exhibits an eclipsed conformation. Because of this, larger columbic repulsion due to torsional strain is expected. Model B (R1(77 K)), however, exhibits a staggered conformation, just as all the fully optimized structures in Figure 6. This may provide an explanation for why the initially formed radical R1-(10 K) is irreversibly transformed to radical R1(77 K) upon slight warming.

4.2. Optimization Procedure and Hyperfine Tensor Calculations of Radical R2. The optimization procedure for model C, mimicking the molecular conformation of radical R2, is done on an SP molecule at the crystallographic structure but without the carboxyl group. Similar to above, the computationally demanding phosphate group has been replaced with hydrogen. Furthermore, one electron is removed from the system making it an oxidation product. An optimization without any geometrical restrictions or modifications is used for model C. As can be seen from Figure 7, the major difference between the unoptimized structure (left) and the optimized structure is the degree of pyrimidalization at the C2 center.

The phosphate group was not reinserted in model C as with models A and B above because by doing this some spin density appeared on the phosphorus atom yielding an isotropic coupling value of −24 MHz, which was not observed experimentally. There is very good agreement between the experimental hyperfine coupling tensors and the corresponding calculated tensors included in Table 3. Evidently, the absence of the phosphate group is not essential for the major results and it appears that Radical R2 most probably is the decarboxylated

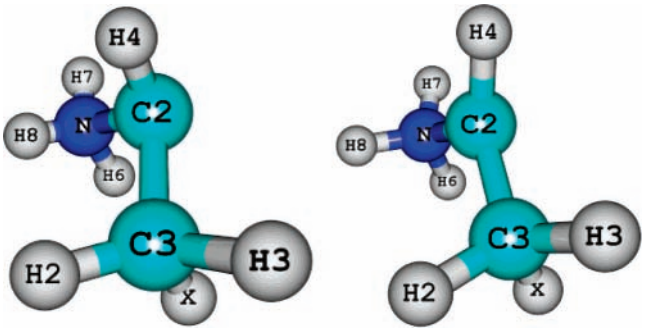

Figure 7. Optimizing the structure to the left gives model C to the right, which is used to calculate the hyperfine coupling tensors for radical R2 formed by X-irradiating L-*O*-serine phosphate single crystals at 10 or 77 K. The x atom is the hydrogen that has replaced the phosphate group. Color coding: C, magenta; H, grey; N, blue.

cation of SP. The calculated spin density at C2 is 0.95, which is in good agreement with the McConnell and Gordy−Bernhard relations discussed earlier (0.90/0.93).

From the discussion above (Section 3.6), tensor no. D could not uniquely be assigned to either H3 or H7. The DFT calculations do not provide any new clues for distinguishing between these two alternatives. Only a successfull ENDOR experiment using partially deuterated crystals can resolve this problem.

4.3. EPR Spectrum Simulations. The hyperfine coupling tensors presented in Tables 1−3 were used for the EPR spectrum simulations of the 10 K experimental data. Furthermore, two additional coupling tensors, which were not experimentally observed from R2 were needed for a satisfactory simulation of the EPR spectrum. The two β protons H2 and H7 or H3, which presumably should give resolvable resonances in the EPR spectra, were not detected in the present ENDOR experiments. As discussed above, either H7 or H3 could be associated with observed tensor no. D. To reproduce the EPR axis-spectra, one additional tensor identical to no. D was used. The second unobserved coupling due to H2 was empirically adjusted to values giving the simulated spectra the correct overall width as compared to experimental spectra. These values were 134, 139, and 115 MHz for the external magnetic field along the crystal axes $\langle a \rangle$, $\langle b \rangle$, and $\langle c \rangle$, respectively, in reasonable agreement with the corresponding values from the DFT calculations (Table 3). These large coupling values explain why this coupling was not observed in the present ENDOR experiments due to the limited range (1−45 MHz) of the rf field scans.

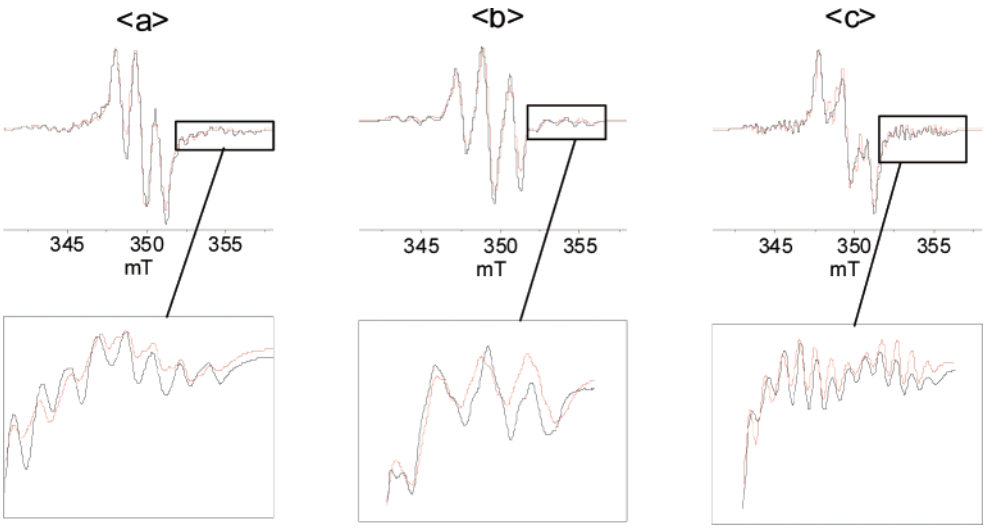

Figure 8. Simulated EPR spectra (red) compared with the experimental EPR spectra (black) from single crystals of L-*O*-serine phosphate X-irradiated and measured at 10 K. The external magnetic field was directed along the three crystallographic axes, as indicated.

The simulated spectra of experiment 10 K shown in Figure 8 reproduce the experimental spectra very well, and it can be concluded that all resolvable resonances in the EPR spectra are due to radicals R1(10 K) and R2.

The EPR spectra from experiment 77 K has a much wider triplet than from experiment 10 K because radical R1(77 K) replaces radical R1(10 K) (Figures 1a, c, and e). These EPR spectra are also reproduced easily by simulation (not shown).

5. Conclusions

Mechanisms for the formation of the three room-temperature radicals R1(295 K), R2(295 K), and R3(295 K) of SP were discussed by Sanderud and Sagstuen.[1] Their proposed primary radicals for two of these room temperature radicals, R1(295 K) and R2(295 K), are those designated R1(10 K)/R1(77 K) and R2 in the present work. In the present work, upon warming above 77 K, radicals R1(77 K) and R2 disappeared and all three previously observed room temperature radicals R1(295 K), R2-(295 K), and R3(295 K) could be observed. Most probably the radicals R1(77 K) and R2 transformed irreversibly into radicals R1(295 K) and R2(295 K), respectively, in agreement with the previous proposals. Upon warming to room temperature after X irradiation at 77 K radical R3(295 K) was detected, but the mechanisms and the precursor for R3(295 K) are still unknown. No phosphate-centered radicals were observed during the present low-temperature experiments; hence, the precursor for the room-temperature radical R3(295 K)[1] appears not to be a phosphoranyl radical as suggested by Lipfert et al.[3]

The observed irreversible umbrella-type inversion of the carboxylic group observed from radical R1(10 K) to R1(77 K) has not been observed previously. The results support the previous assumptions on pyramidal carboxylic anions mainly derived from ^{13}C hyperfine coupling tensors.[4] However, the present results seem to indicate that the constants (in particular B_2) in eq 3 need to be revised because an isotropic coupling from a hydroxylic β-proton coupling (no. II) was observed, which cannot be described properly by this equation.

Acknowledgment. Drs. Anders Lund and William H. Nelson are acknowledged for providing their computer programs KVASAT and MAGRES, respectively, and for helpful discussions.

References and Notes

(1) Sanderud, A.; Sagstuen, E. *J. Phys. Chem.* **1996**, *100*, 9545.
(2) Sagstuen, E.; Sanderud, A.; Hole, E. O. *Radiat. Res.* **2004**, *162*, 112.
(3) Lipfert, J.; Llano, J.; Eriksson, L. A. *J. Phys. Chem. B* **2004**, *108*, 8036.
(4) Muto, H. Trapped Anions In Organic Crystals. In *Radical Ionic Systems: Properties in Condensed Phases*; Lund, A., Shiotani, M., Eds.; Kluwer Academic Publishers: 1991; Vol. 6.
(5) Sundaralingam, M.; Putkey, F. F. *Acta Crystallogr., Sect. B* **1970**, *B26*, 790.
(6) Schonland, D. S. *Proc. Phys. Soc.* **1959**, *73*, 788.
(7) Nelson, W. H. *J. Magn. Reson.* **1980**, *38*, 71.
(8) Sørnes, A. R.; Sagstuen, E.; Lund, A. *J. Phys. Chem.* **1995**, *99*, 16867.
(9) Sørnes, A.; Sagstuen, E. *J. Phys. Chem.* **1995**, *99*, 16857.
(10) Sagstuen, E.; Lund, A.; Itagaki, Y.; Maruani, J. *J. Phys. Chem. A* **2000**, *104*, 6362.
(11) Sagstuen, E.; Hole, E. O.; Haugedal, S. R.; Lund, A.; Eid, O. I.; Erickson, R. *Nukleonika* **1997**, *42*, 353.
(12) Frisch, M. J.; Trucks, G. W.; Schlegel, H. B.; Scuseria, G. E.; Robb, M. A.; Cheeseman, J. R.; Montgomery, J. A., Jr.; Vreven, T.; Kudin, K. N.; Burant, J. C.; Millam, J. M.; Iyengar, S. S.; Tomasi, J.; Barone, V.; Mennucci, B.; Cossi, M.; Scalmani, G.; Rega, N.; Petersson, G. A.; Nakatsuji, H.; Hada, M.; Ehara, M.; Toyota, K.; Fukuda, R.; Hasegawa, J.; Ishida, M.; Nakajima, T.; Honda, Y.; Kitao, O.; Nakai, H.; Klene, M.; Li, X.; Knox, J. E.; Hratchian, H. P.; Cross, J. B.; Bakken, V.; Adamo, C.; Jaramillo, J.; Gomperts, R.; Stratmann, R. E.; Yazyev, O.; Austin, A. J.; Cammi, R.; Pomelli, C.; Ochterski, J. W.; Ayala, P. Y.; Morokuma, K.; Voth, G. A.; Salvador, P.; Dannenberg, J. J.; Zakrzewski, V. G.; Dapprich, S.; Daniels, A. D.; Strain, M. C.; Farkas, O.; Malick, D. K.; Rabuck, A. D.; Raghavachari, K.; Foresman, J. B.; Ortiz, J. V.; Cui, Q.; Baboul, A. G.; Clifford, S.; Cioslowski, J.; Stefanov, B. B.; Liu, G.; Liashenko, A.; Piskorz, P.; Komaromi, I.; Martin, R. L.; Fox, D. J.; Keith, T.; Al-Laham, M. A.; Peng, C. Y.; Nanayakkara, A.; Challacombe, M.; Gill, P. M. W.; Johnson, B.; Chen, W.; Wong, M. W.; Gonzalez, C.; Pople, J. A. *Gaussian 03*, revision B.04; Gaussian, Inc.: Wallingford, CT, 2004.
(13) Becke, A. D. J. *J. Chem. Phys.* **1993**, *98*, 5648.
(14) Lee, C.; Yang, W.; Parr, R. G. *Phys. Rev. B* **1988**, *37*, 785.
(15) Stevens, P. J.; Devlin, F. J.; Chabalowski, C. F.; Frisch, M. J. *J. Phys. Chem.* **1994**, *98*, 11623.
(16) Frisch, Æ.; Frisch, M. J. *Gaussian 98 User's Reference*, Second ed.; 1999.
(17) Ban, F.; Gauld, J. W.; Wetmore, S. D.; Boyd, R. J. The Calculation of the Hyperfine Coupling Tensors of Biological Radicals. In *Progress in Theoretical Chemistry and Physics: EPR of Free Radicals in Solids*; Lund, A., Shiotani, M., Eds.; Kluwer Academic Publishers: Dordrecht, 2003; Vol. 10.
(18) Cramer, C. J. *Essentials of Computational Chemistry. Theories and Models*, 2nd ed.; John Wiley & Sons: England, 2004.
(19) Vanhaelewyn, G.; Jansen, B.; Pauwels, E.; Sagstuen, E.; Waroquier, M.; Callens, F. *J. Phys. Chem. A* **2004**, *108*, 3308.
(20) Reed, A. E.; Weinstock, R. B.; Weinhold, F. *J. Chem. Phys.* **1985**, *83*, 735.
(21) Muto, H.; Nunome, K.; Iwasaki, M. *J. Chem. Phys.* **1974**, *61*, 1075.

(22) Muto, H.; Nunome, K.; Iwasaki, M. *J. Chem. Phys.* **1974**, *61*, 5311.
(23) Muto, H.; Iwasaki, M. *J. Chem. Phys.* **1973**, *59*, 4821.
(24) Iwasaki, M.; Muto, H. *J. Chem. Phys.* **1974**, *61*, 5315.
(25) Miyagawa, I.; Tamura, N.; Cook, J. W., Jr. *J. Chem. Phys.* **1969**, *51*, 3520.
(26) McConnell, H. M. *J. Chem. Phys.* **1965**, *24*, 764.
(27) Fessenden, R. W.; Schuler, R. H. *J. Chem. Phys.* **1963**, *39*, 2147.
(28) Gordy, W. *Theory and Application of Electron Spin Resonance*; John Wiley & Sons: New York, 1980.
(29) Bernard, W. A. *J. Chem. Phys.* **1984**, *81*, 5928.
(30) Erling, P. A.; Nelson, W. H. *J. Phys. Chem. A* **2004**, *108*, 7591
(31) Heller, C.; McConnell, H. M. *J. Chem. Phys.* **1960**, *32*, 1535.
(32) Morton, J. R. *Chem. Rev.* **1964**, *64*, 453
(33) Sagstuen, E.; Hole, E. O.; Haugedal, S. R.; Nelson, W. H. *J. Phys. Chem. A* **1997**, *101*, 9763.
(34) Sanderud, A.; Sagstuen, E. *J. Phys. Chem. B* **1998**, *102*, 9353.
(35) Chen, Y.; Close, D. *THEOCHEM* **2001**, *549*, 55.